Fractographical Analysis of Fish-eye Formation
under Multiaxial Fatigue

Štěpán Major[1a], Karel Slámečka[1b], Marta Kianicová[2c] and Jaroslav Pokluda[1d]

[1]Institute of Engineering Physics, Brno University of Technology, Technická 2,
616 69 Brno, Czech Republic

[2]Faculty of Special Technology, Alexander Dubcek University in Trenčín, Študentská 1,
911 50 Trenčín, Slovakia

[a]ymajor02@stud. fme.vutbr.cz, [b]slamecka@fme.vutbr.cz, [c]kianicova@tnuni.sk,
[d]pokluda@fme.vutbr.cz

Keywords: Plasma nitriding; Fatigue life; Fatigue fracture; Fish-eye crack; Multiaxial loading.

   Abstract. This work deals with fractographical analysis of fish-eye crack formation under multiaxial fatigue. In this work, it is shown that the subsurface fish-eye type crack formation is the typical fatigue crack initiation mechanism in nitrided steels and the mechanism of subsurface nucleation was studied. Dependence between type of loading characterized by loading ratio $z = \tau_a / (\tau_a + \sigma_a)$ (σ_a is the bending amplitude and τ_a is the torsion amplitude) or number of cycles to failure and geometrical characteristics of fish-eye crack was studied. Moreover, Stress intensity factors for fish-eye crack were assessed.

Introduction

The machine components working under cyclic loads are severely subjected to the threat of fatigue failure. Some thermo-chemical surface treatments such as nitriding improve the fatigue performance of machine components. Fatigue life improvement is caused by generation of high compressive residual stresses below the surface of machine parts. Low tensile residual stresses are introduced in the core [1-9]. Plasma nitriding is a process already consolidated in industry, being used in improvements of several physical properties in metallic surfaces, like hardness or corrosion strengths, resulting in increasing useful life of mechanical component [1-12]. The long life of nitrided specimens corresponds to the fracture initiation below the nitrided layer. Long life fractures usually reveal two remarkable features: a) crack nucleation on the nonmetallic inclusion, b) propagation of a crack inside the specimen in vacuum forming the so-called fish-eye crack, see Fig. 1. Majority of published investigations deals with dependence between fatigue life of specimens and the depth of the nitride layer [1, 2, 9]. However, all these investigations deals only with the pure-bending loading.

   In the center of the fish-eye crack, an inclusion is found and in the case of ultralong life ($N_f > 10^7$) there is the optically different region in its vicinity [12,13]. Murakami et al. termed this area as "optically dark area" (ODA), which coincides with the "granular-brightfacet" zone observed by Shiozawa et al. [14]. In case of ultralong life, ODA is formed by hydrogen-trapped fatigue. The fish-eye is typical for fracture surface of nitrided specimens; in the case of virgin specimen fish-eye cannot be found within specimen failed at a small number of cycles [12,13]. According to SEM observations, ODA has a very rough fracture surface that is quite different from that of the area outside ODA, which shows a fatigue fracture surface typical of the structure of a martensite lath [12, 13]. Inside of the fish-eye region, the crack looks white to the naked eye or under optical microscope, whereas the region outside the fish-eye looks grey. This difference in color is caused by different fracture mechanisms. The white surface inside the fish-eye crack is caused by cyclic contact of the fracture surfaces in the absence of atmospheric effects within the fish-eye crack. The grey region outside the fish-eye is produced by static fracture or quasi-static fracture (in the case of

fracture surface formed by cyclic contact of the fracture surfaces in the presence of atmospheric effects) for bending loading. In the case of rotating-bending (with supremacy of rotating loading), the presence of atmospheric effects in fracture surface formation is more significant [15].

Specimens and Fatigue experiments

Material characterization. Chemical composition of the based material, the steel EN 37CrAlMo 6 is: C 0.357%; Mn 0.468%; Cr 1.49%; Mo 0.194%; V 0.01%; Cu 0.072%; Al 1.40%; W 0.032%; Si 0.292%; P 0.006%; S 0.005% and Fe as remainder. When compared with commonly treated nitriding steels, the investigated steel has a slightly higher percentage of carbon. It offers higher values of strength but simultaneously introduces higher differences in microstructure resulting from variations in nitriding procedures.

Plasma nitriding, also called ion nitriding, is wide-spread surface hardening process utilized to improve the mechanical properties. Technology of plasma nitriding has been described in earlier reports [1-7]. This technology is characterized by adsorption of nitrogen atoms on the surface in the form of N^+ ions or NH^+, NH_2^+ and NH_3^+ ions. Owing to the low energy up to 10 eV, there is no implantation of N atoms and the nitrogen transport from the surface into the bulk is accomplished by the mechanism of an interstitial diffusion. Layers of different depth of nitrogen penetration and of different phase compositions can be realized in this way. An important parameter, determining the fatigue strength of nitrided parts, is the thickness of the surface layer. The structure of the plasma nitrided layer consists basically of diffusion and compound layer (white layer). The latter one is composed of different iron nitride phases Fe_4N (γ') and Fe_3N (ε) nitrides. Parameters of the applied nitriding process are presented in Table 1.

Table 1. Parameters of nitriding.

STEP	t_{in} [°C]	*Time* [h]	*Atmosphere*			*Press.* [Pa]	*U* [V]	*Puls* [μs]
			N_2	H_2	CH_4			
cleaning	510	0:30	20	2		$7 \cdot 10^5$	800	120
nitriding	515	32:00	21	7	0.4	$2.6 \cdot 10^5$	530	150

Mechanical properties of nitrided material are: $R_{p\,0.2}$ = 871 MPa and R_m = 1020 MPa, HV_{max} = 1280 on the surface, the depth of nitride layer h_{nitr} =200 μm . Tensile strength properties of tempered steel (before nitriding) were: $R_{p\,0.2}$ = 839 MPa and R_m = 954 MPa, i.e. slightly lower in comparison with the strength of nitrided specimens.

Fatigue experiments. Fatigue experiments were performed using the resonance testing machine MZGS-100. Twenty-five smooth specimens were loaded until final failure. Bending and torsion loadings (frequency 29 Hz, R = -1) and their synchronous in-phase combinations were applied at room temperature.

Measured parameters

Geometry of Fish-eye crack. Region of crack initiation (Fish-eye crack) and all measured characteristic are schematically shown in Fig. 1b. These characteristics were measured with optical instrument FRT MicroProf 100 for all studied specimens. The size of inclusion was measured by stereophotogrammetry.

Reconstruction of fracture surface. The detailed reconstruction of fracture surface of five specimen was obtain by stereophotogrammetry. Stereophotogrammetry is based on the software evaluation of two digitalized images of fracture surface taken from different positions [16]. Stereophotoimages of selected parts of surface on each specimen were acquired using SEM and the tilting angle of stereopairs was 10°. The commercial software MeX was used for data processing.

The output of the procedure is the digital elevation model of depicted surface region consisting of up 30.000 points.
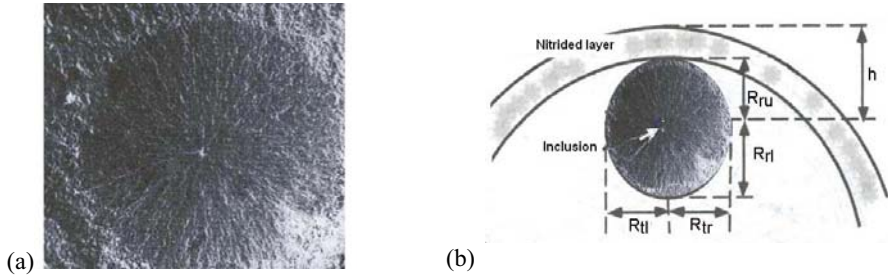

(a)

(b)

Fig. 1 (a) Micrograph of the fish-eye crack, (b) schema of Fish-eye crack.

Experimental results. The analysis of crack initiation show three distinct regions, the optically clearly visible dark centre, the so-called ODA or pure inclusion [12], the white region fish-eye crack and rough optically grey threshold, see Fig.1a. Fig. 2a shows dependence between average value of Fish-eye crack radius R_{avr} ($R_{avr}= (R_{tl} + R_{tr} + R_{ru} + R_{rl})/4$) and the loading ratio and Fig. 2b show the dependence between R_{avr} and the number of cycles to failure. Fig. 2c shows the fish-eye size R_{avr} as a function of depth of the inclusion below specimen surface, h.
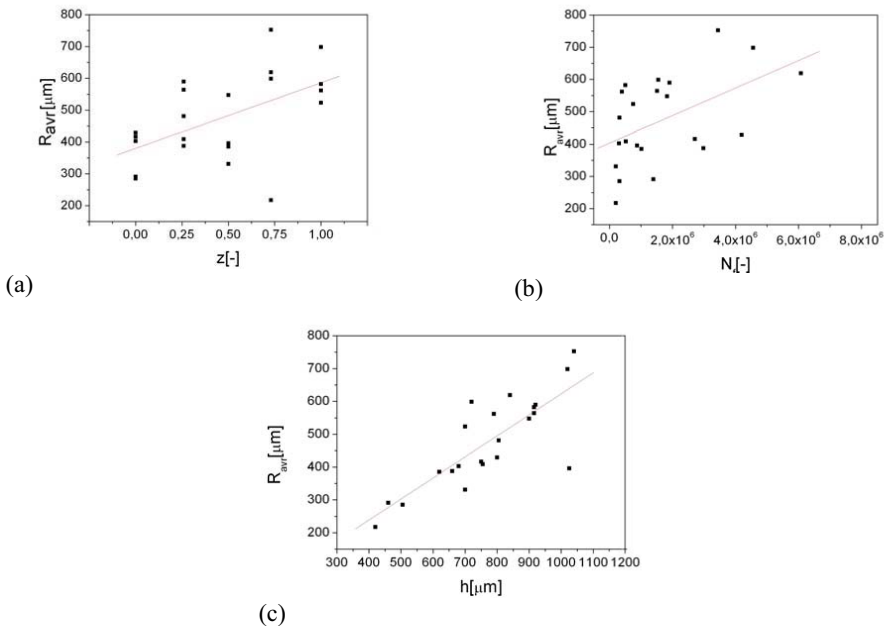

(a)

(b)

(c)

Fig. 2 (a) Dependence between R_{avr} and the loading ratio, z, (b) dependence between R_{avr} and N_f, (c) R_{avr} as a function of the depth of the inclusion below specimen surface, h.

Generally, the fish-eye is not symmetrical. The asymmetry S_V defined as ratio R_{vu}: R_{vl} depend on the depth h, as is shown in Fig. 3a. In the case of prevailing torsion-loading, both vertical radii R_{ru}

and R_{rl} and horizontal radii R_{tr} and R_{tl} are asymmetrical, with the laters having evidently higher values, see Fig. 3b. The Fig. 3b shows dependence between elliptical coefficient Q and loading ratio z, elliptical coefficient Q is defined as $Q = (R_{tl} + R_{tu})/(R_{ru} + R_{rl})$. This effect is caused by a higher crack growth rate in the mode II (tangential) than that in the mode III (radial) as already reported in [17]. The asymmetry of fish-eye in the vertical direction is caused by the difference in net stress and material strength between the crack propagating towards the surface compared to the crack propagating nearer the center of specimen [2]. For inclusions located at less than h_l limit measure of depth ($h_l = 550\mu m$, see Fig. 3a), the crack front growing from the inclusion-matrix interface toward the center or in the horizontal direction can propagate faster than cracks growing towards the nitride layer.
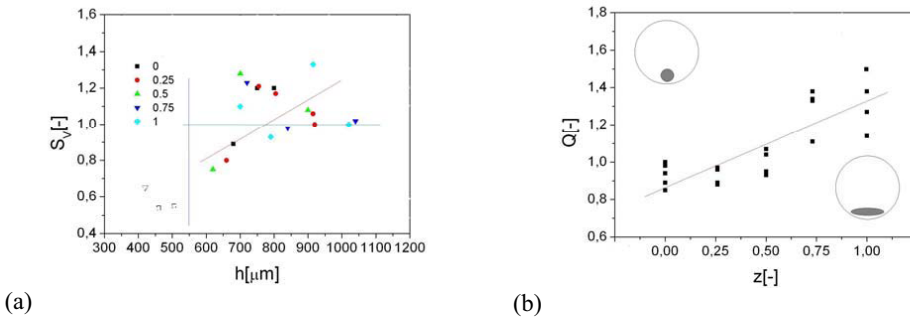

(a)   (b)

Fig. 3 (a) Dependence between coefficient of asymmetry, S_V, and the position below specimen surface, h, (b) dependence between elliptical coefficient, Q, and the loading ratio, z.

Fig. 4 showed profiles cutting the fish-eye crack in the radial and tangential direction. The height and roughness is steady increasing with the distance from the center of the crack (inclusion) and the roughness sudden increase in the grey region represents the threshold of the Fish-eye crack. These two regions represent two distinct type of crack growths [12]. Higher value of vertical roughness R_V (average value in radial direction 8.93µm and 7.14 µm in tangential direction) in radial direction is can be explained by presence of micro-mode III.

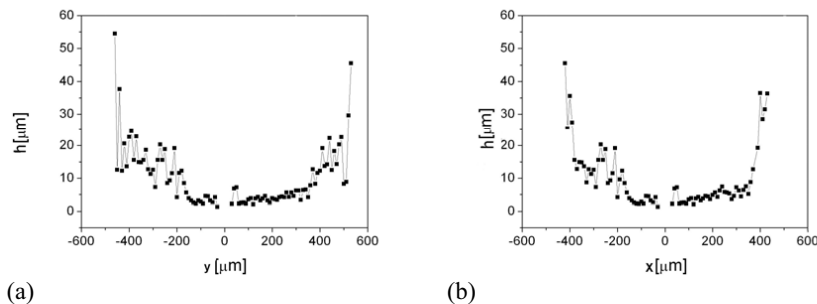(a)   (b)

Fig. 4. Dependence between profile height, and the distance from inclusion, x,y.
(a) Radial direction. (b) Tangential direction.

Fracture mechanics

It is quite common for heat-treated materials to have high residual stress, which inhibits the formation of the crack on the surface and allows formation of internal crack more deeply in the core. Theoretical distribution of threshold value of stress intensity factor, K_{th}, and the critical diameter of inclusion, d_{ef}, in material with nitrided layer were calculated in Pokluda at al. [8], see Fig.5. The critical dimension inside the nitrided layer exceeds, by two orders of magnitude, the inclusion size of tens of μm commonly found in commercial steels. This is the reason why there is no crack initiation observed on inclusions inside the nitrided layers. On the other hand, d_{ef} of an inclusion in the core (in the depth more than 0.5 mm from the specimen surface) fully corresponds to a observed dimension of inclusions.
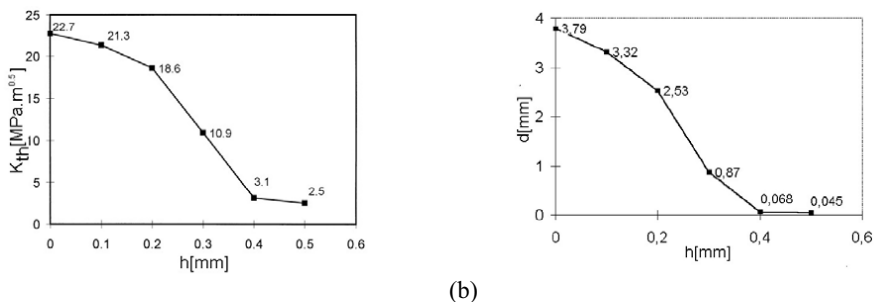

(a) (b)

Fig. 5 (a) Distribution of K_{th} in nitrided layer (from [8]) and
(b) critical dimension of inclusion (from[8]).

Table 2. Parameters of analyzed Fish-eye crack.

σ_a [MPa]	N_f [-]	h [μm]	d [μm]	R_{ru} [μm]	R_{rl} [μm]	R_{tl} [μm]	R_{tr} [μm]
650	4198000	800	44	510	420	425	420

For one specimen fractured by pure bending, stress intensity factors at points A and B (see Fig. 6a) were calculated at start of growth and at the moment of final fracture. Parameters of fractured specimen are shown in Table 2. Stress intensity factors were calculated by formula:

$$K_{IA,B} = \left\{ \frac{1}{1.569}\frac{s}{R} \pm 0.4246\frac{b}{R} \right\}\sigma_a\sqrt{\pi b} \,,$$

where $b = R_{ru}$ for K_{IA} and $b = R_{rl}$ for K_{IB} and $R = 4\text{mm}$ is radius of specimen. Calculated values of the stress intensity factor are K_{I0A}= 2.8 MPa√m, and K_{I0B}= 2.7 MPa√m at the inclusion diameter (onset of growth) and K_{IA}= 11.8MPa√m, K_{IB} = 13.1MPa√m at the moment of final fracture. The latter values seem to be small for final rapture of the specimen. On the fracture surface, second small surface crack c mutual distance loosed to the studied fish-eye crack was observed. If the distance of these two cracks is smaller than the size of smaller crack (see. Fig. 6b, compare distance KL and LM), stress intensity factor K_I at point M and L increases significantly, and cracks near to each other are likely to coalesce in the manner of unstable rupture [15]. This effect explains also the existence of an high step 50μm of on the border of fish-eye crack, see Fig. 4. Indeed both coagulating cracks are obviously growing in two different planes, approximately 50μm of mutual distance.
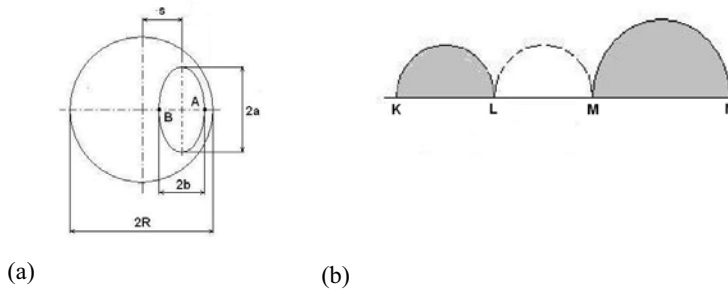
(a) (b)

Fig. 6 (a) The fish-crack modeled as the elliptical crack,
(b) interaction effect between adjacent cracks.

Summary

The average value of fish-eye crack radius increases with the number of cycles to failure, the depth of inclusion below the specimen surface and the loading ratio, z. The coefficient of asymmetry S_V shows that the internal cracks in the vicinity of the nitrided layer are distinctively asymmetric (influence of residual compressive stresses), because the crack grows into the core of the specimen more easily than into the zone affected by nitride layer. The shape of the fish-eye changes from a circle to an ellipse with increasing portion of the torsion component. This effect is explained by the fact that the fish-eye crack growth is faster in the tangential direction under mode II than that in the radial direction under the less effective mode III. The extremely high step on the border of the fish-eye crack on analyzed specimen can be explained by propagation of two cracks in two different planes and their coalescence in the manner of unstable fracture.

References

[1] K. Genel, M. Demirkol and M. Çapa, Materials Science and Engineering A, Volume 279, Issues 1-2, 29, 2000, p. 207.

[2] P. De la Cruz, M. Oden and T. Ericsson, Materials Science and Engineering A, Volume 242, 1998, p. 181.

[3] Metals Handbook, Vol. 4, Heat Treating, 9th edition, American Society for Metals, Metals Park, OH, 1991, p. 387.

[4] K.E. Thelning, Steel and Its Heat Treatment, Bofors Handbook, Butterworths, London, 1975, p. 377.

[5] H. J. Spies, Steel Res. 64 (1993), p. 441.

[6] B. Edenhoffer, Engineering Bookshelf, Source Book on Nitriding, American Society for Metals, Metals Park OH, 1977, p.181.

[7] J. M. Cowling and J.W. Martin, Met. Technol. 8, 1981, 289.

[8] J. Pokluda, I. Dvořák, H. Horáková and Š. Major: In: "Fatigue 06", Ed. W. S. Johnson, Elsevier (CD), Atlanta, Georgia, 2006, p. 0601A_24.

[9] A. Alsaran, M. Karakan and A. Çelik, Materials Characterization 48, 2002, pp.323.

[10]   C.K. Jones, S.W. Martin, D.J. Sturges and M. Hudis, Ion nitriding, in: Heat Treatment, vol. 73, The Metal Society, London, 1973, pp.71–77.

[11]   B. Edenhofer, Heat Treat. Met. 1 (2), 1974, 56–67.

[12]   M. D. Chapetti, T. Tagawa, T. Miyata, Materials Science and Engineering A, Volume 356, Issues 1-2, 15 September 2003, pp. 227-235

[13]   Y. Murakami, T. Nomoto, T. Ueda, Fatigue Fract. Eng. Mater.Struct. 22, 1999, pp. 581-590.

[14]   K. Shiozawa, L. Lu, S. Ishihara, Fatigue Fract. Eng. Mater. Struct. 24, 2001, pp. 781-790.

[15]   Y. Murakami, Metal Fatigue: Effects of Small Defects and Nonmetallic Inclusions, Elsevier 2002.

[16]   S. Scherrer, O. Kolednik, Europ. Microsc. Analysis., March 2001, pp.15-17.

[17]   J. Pokluda, G. Trattnig, C. Martinschitz, R. Pippan: Int. J. Fatigue 30, 2008, pp. 1498 – 1506.